CHEMISTRY

Mechanism for selective binding of aromatic compounds on oxygen-rich graphene nanosheets based on molecule size/polarity matching

Heyun Fu[1]†, Bingyu Wang[1,2]†, Dongqiang Zhu[3]*, Zhicheng Zhou[1], Shidong Bao[1], Xiaolei Qu[1], Yong Guo[4], Lan Ling[5], Shourong Zheng[1], Pu Duan[6], Jingdong Mao[7], Klaus Schmidt-Rohr[8], Shu Tao[3], Pedro J. J. Alvarez[9]

Selective binding of organic compounds is the cornerstone of many important industrial and pharmaceutical applications. Here, we achieved highly selective binding of aromatic compounds in aqueous solution and gas phase by oxygen-enriched graphene oxide (GO) nanosheets via a previously unknown mechanism based on size matching and polarity matching. Oxygen-containing functional groups (predominately epoxies and hydroxyls) on the nongraphitized aliphatic carbons of the basal plane of GO formed highly polar regions that encompass graphitic regions slightly larger than the benzene ring. This facilitated size match–based interactions between small apolar compounds and the isolated aromatic region of GO, resulting in high binding selectivity relative to larger apolar compounds. The interactions between the functional group(s) of polar aromatics and the epoxy/hydroxyl groups around the isolated aromatic region of GO enhanced binding selectivity relative to similar-sized apolar aromatics. These findings provide opportunities for precision separations and molecular recognition enabled by size/polarity match–based selectivity.

INTRODUCTION

Selective molecular binding of organic compounds finds many important applications in the fine chemical and pharmaceutical industries, such as separation of close-boiling organic isomers, selective catalytic reactions, purification and recovery of valuable chemicals, and drug delivery (*1*–*4*). Precise separation of different xylenes is a classic example, in which *p*-xylene is the most desirable chemical as it is the feedstock for the production of other valuable products (*5*, *6*). A broad group of framework materials with uniform, molecular-scale pore structures, including zeolites, metal-organic frameworks, and covalent-organic frameworks, have been developed to achieve chemical separation via molecular sieving (*7*–*12*). However, these materials often suffer from slow separation/conversion kinetics because of severe limitations associated with micropore diffusion, especially when the size of molecules is close to the pore size (*8*, *11*).

Engineered carbon nanomaterials (CNMs), including carbon nanotubes (CNTs), graphenes, and graphene oxides (GO), show great potential for selective binding of organic chemicals in broad applications, including chemo- and biosensors, analyte preconcentration, and water and wastewater treatment (*13*–*18*). The large specific surface area combined with the high hydrophobicity and electronically delocalized graphitized carbons (fused aromatic rings) of CNMs facilitates the binding of hydrophobic organic chemicals, particularly those that can induce π-π electron coupling interactions, from aqueous solution (*17*, *18*). The surface chemistry of CNMs can be fine-tuned to enhance their binding affinity toward target organic chemicals. Oxygen-functionalized CNTs exhibit a stronger binding affinity for amino-substituted aromatic compounds owing to enhanced π-π electron coupling interactions and extra Lewis acid-base interactions compared to nonsubstituted counterparts (*19*). Another example is that functionalization of GO with sulfonate groups creates conjugate π-region sites and negatively charged edge sites simultaneously, which are highly exposed and available for binding phenanthrene and methylene blue, respectively (*20*). In addition, doping heteroatoms (e.g., N or B) into the graphitic lattice of CNMs can polarize more abundant electron-depleted sites around the doped atoms, facilitating π-π electron-donor-acceptor interactions with π-electron-donor compounds (e.g., aromatics substituted with electron-donating groups such as hydroxyl and amine) (*21*, *22*). However, achieving high molecular selectivity by adsorption on CNMs is a pervasive challenge that limits related applications in precision separation and molecular recognition.

Here, we report the size match– and polarity match–based binding between aromatic compounds and basal-plane oxygen-enriched GO, leading to high selectivity and precision separation of target molecules with complementary size and polarity. We investigate the binding affinity of four groups, a total of 21 aromatic compounds, on oxygen-enriched GO in an aqueous solution and find pronounced selectivity of GO for small apolar molecules and similar-sized polar molecules. Molecular binding selectivity is also examined in the gas phase for selected compounds. Experimental and density functional theory (DFT) calculation results indicate that the selectivity of GO is primarily due to the size match–based interactions between aromatics and graphitic regions and is tuned by the

[1]State Key Laboratory of Pollution Control and Resource Reuse, School of the Environment, Nanjing University, Jiangsu 210023, China. [2]School of Environmental and Biological Engineering, Nanjing University of Science and Technology, Jiangsu 210094, China. [3]Key Laboratory of the Ministry of Education for Earth Surface Processes, School of Urban and Environmental Sciences, Peking University, Beijing 100871, China. [4]Key Laboratory of Integrated Regulation and Resource Development on Shallow Lakes of Ministry of Education, College of Environment, Hohai University, Jiangsu 210098, China. [5]State Key Laboratory of Pollution Control and Resource Reuse, College of Environmental Science and Engineering, Tongji University, Shanghai 200092, China. [6]Department of Chemistry, Massachusetts Institute of Technology, Cambridge, MA 02139, USA. [7]Department of Chemistry and Biochemistry, Old Dominion University, Norfolk, VA 23529, USA. [8]Department of Chemistry, Brandeis University, Waltham, MA 02453, USA. [9]Department of Civil and Environmental Engineering, Rice University, Houston, TX 77005, USA.
*Corresponding author. Email: zhud@pku.edu.cn
†These authors contributed equally to this work.

compatibility between molecule polar groups and oxygen functional groups encompassing the graphitic regions of GO.

RESULTS

Small graphitic patches on the GO surface isolated by C—O moieties

The GO used in this study was prepared from graphite flakes by the widely used Hummers chemical oxidation method (*18*, *23*). The GO surface was rich in oxygen [33 atomic % (at %)] in the form of epoxy and hydroxyl groups, as revealed by the x-ray photoelectron spectroscopy (XPS) and Fourier transform infrared analysis (fig. S1, A and B). Because of these oxygen functional groups, GO has a relatively large interlayer spacing of 0.90 nm [determined from the (001) peak at $2\theta = 9.8°$ in the x-ray diffraction pattern; fig. S1C]. The intensity ratio of Raman D-band to G-band (i.e., I_D/I_G) is 0.91 (fig. S1D), suggesting the presence of a high content of functional groups (*24*, *25*). The average size of the graphitic regions of GO was calculated to be 4.8 nm using the empirical Tuinstra-Koenig relation (*26*). As revealed by transmission electron microscopy (TEM) combined with atomic force microscopy (fig. S1, E and F), GO has relatively intact and smooth two-dimensional atomic sheets with few defects or holes.

To gain a deeper insight into its structural characteristics, we further characterized the GO using high-resolution (HR)–TEM and solid-state ^{13}C nuclear magnetic resonance (NMR). GO consists of a substantial amount of well-crystallized graphitic regions with a clear hexagonal lattice (Fig. 1C), as shown in the HR-TEM images, which are isolated by regions of amorphous carbons (Fig. 1B). These amorphous carbons are most likely the oxidized carbons in GO (*25*, *27*, *28*). The size of the graphitic regions in the HR-TEM images is in the range of 2.5 to 5.6 nm, in agreement with the average size determined by the Raman analysis. Figure 1D presents the quantitative ^{13}C direct polarization NMR spectrum of GO. The spectrum is dominated by three peaks at 62, 71, and 131 parts per million (ppm), which are assigned to carbons in epoxy (C—O—C), hydroxyl (C—OH), and aromatic rings, respectively (*29*–*32*). We also observed three minor peaks corresponding to carbons in lactol (O—C—O) (at 101 ppm) (*31*) and carboxyl (COOH) at the edge of graphene sheets (at 166 ppm) (*32*), and carbonyl (C═O) bonded to aromatic rings (at 188 ppm) (*29*). This is typical of ^{13}C NMR spectra for GO samples prepared from chemical oxidation methods (*29*–*32*). The content of different carbon species was determined on the basis of the integrated intensities of the NMR peaks (table S1). The GO contains approximately 29% of aromatic carbons, 30% of C—O—C, 26% of C—OH, 5% of COOH, 5% of aromatic C═O, and 4% of O—C—O. The content ratio of COOH to C—OH is 19%, generally agreeing with the previously reported ratio for GO (*30*). In summary, the GO used in the present study is mainly composed of small graphitic regions (size of 2.5 to 5.6 nm) that are isolated by sp^3-hybridized C—O moieties (i.e., C—OH and C—O—C) (Fig. 1E).

Size selectivity of aromatics on oxygen-enriched GO in aqueous phase

First, we examined the selective binding ability of GO for various aromatic compounds [benzene, polycyclic aromatic hydrocarbons (PAHs), and chloro-, methyl-, nitro-, hydroxyl-, and/or amino-substituted

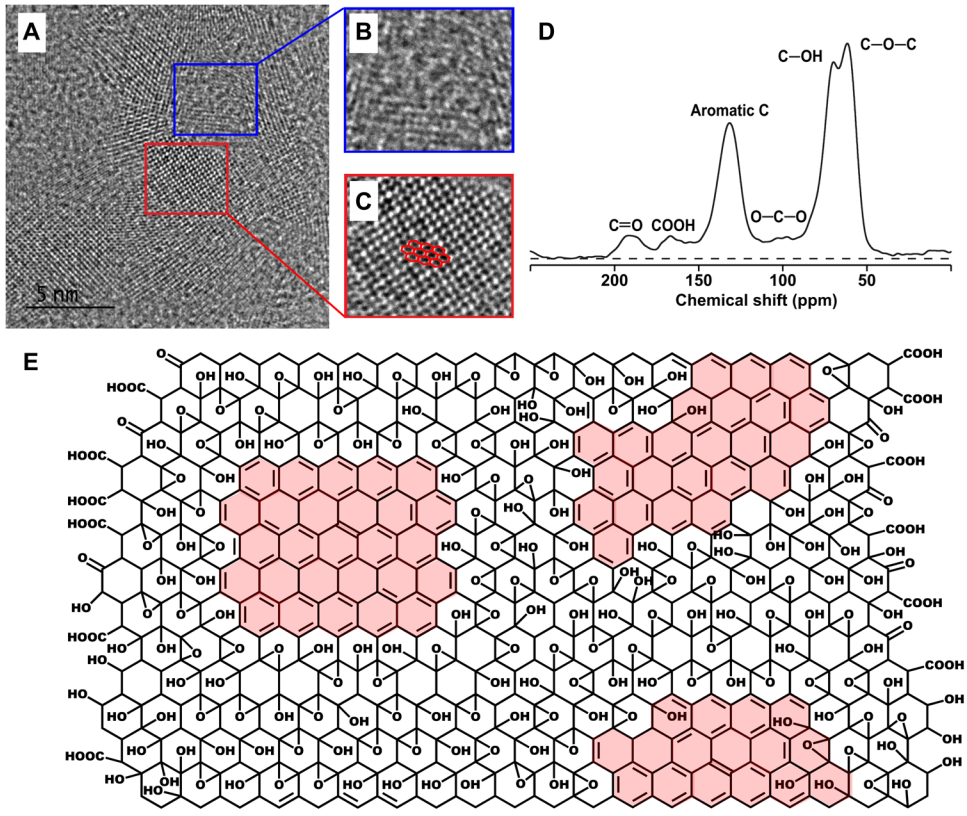

Fig. 1. Chemical structures of GO. (**A**) HR-TEM image and (**B** and **C**) the enlargements, as marked, of GO. (**D**) Solid-state ^{13}C direct polarization NMR spectrum of GO. (**E**) Schematic structure of GO. Red areas indicate the isolated graphitic regions.

benzenes/naphthalenes] in aqueous solution using batch adsorption experiments. The chemical structures and molecular sizes of these compounds are presented in fig. S2, and their selected physical-chemical properties are listed in table S2. The single-solute adsorption isotherms are shown in Fig. 2. The Freundlich model was adopted to fit the adsorption data as it provided the best fitting ($R^2 > 0.93$ for most tested compounds; fitting results are presented in table S3). The distribution coefficient (K_d, liter/kg; table S3) was calculated from the sorption model at a selected aqueous-phase concentration (C_e) from the middle of the isotherm concentration ranges, and the corresponding adsorbed amount (q_e) did not exceed the maximum for monolayer adsorption.

GO exhibits remarkably enhanced binding for small molecules. For example, at the same selected C_e (0.004 mM), the K_d of benzene is more than 10 times higher than that of naphthalene, and the enhancement is even larger (~30 times) when compared with phenanthrene. Similar size selectivity is also observed with the three groups of methyl-, chloro-, and nitro-substituted benzenes. The K_d of toluene, chlorobenzene, and nitrobenzene is on the order of 10^3 to 10^5 liters/kg, approximately one order of magnitude higher than that of most tested multisubstituted benzenes (e.g., dichlorobenzenes, *o*-xylene, 1,2,4-trichlorobenzene, 1,3,5-trichlorobenzene, 1,3,5-trimethylbenzene, and 1,3,5-trinitrobenzene). The size selectivity of GO was further probed with binary-solute adsorption experiments (fig. S3). In all the tested binary-solute systems (benzene/naphthalene, benzene/phenanthrene, toluene/*o*-xylene, toluene/1,3,5-trimethylbenzene, chlorobenzene/*o*-dichlorobenzene, and chlorobenzene/1,3,5-trichlorobenzene), GO consistently exhibited higher affinity for the smaller aromatic molecules (indicated by K_d values). The presence of larger aromatics had little influence on the binding affinity of GO for smaller aromatics. These observations confirm the size-based selectivity of GO. The binding of apolar organic compounds to carbonaceous materials is mostly controlled by hydrophobic interactions (*17*, *18*). For the tested apolar aromatics (benzene, PAHs, and chloro- and methyl-substituted benzenes), the hydrophobicity [quantified by water solubility (S_W) and *n*-octanol–water partition coefficient (K_{OW}); table S2] increases with molecular size. Thus, the binding selectivity of GO for the small apolar aromatics would be even more pronounced if the effect of hydrophobicity is considered.

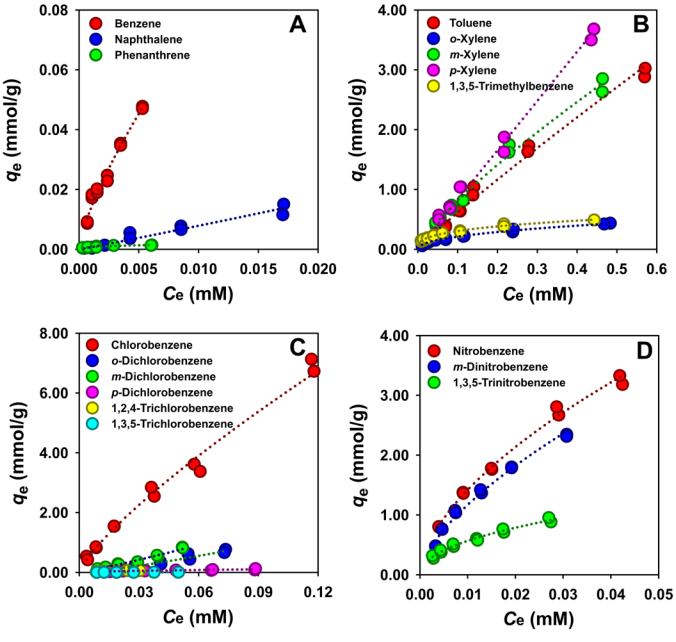

Fig. 2. Binding affinity of aromatics with different sizes on GO in the aqueous phase. Adsorption isotherms plotted as adsorbed concentration (q_e) against aqueous-phase concentration (C_e) at equilibrium for (**A**) benzene and PAHs, (**B**) methyl-substituted benzenes, (**C**) chloro-substituted benzenes, and (**D**) nitro-substituted benzenes. The experiments were conducted using a batch approach at ambient temperature. All adsorption data were collected in duplicate.

Polarity selectivity of aromatics on oxygen-enriched GO in aqueous phase

An interesting finding is that GO exhibits lower size selectivity for the polar nitro-substituted benzenes than the three groups of apolar aromatic compounds (Fig. 2). For example, although 1,3,5-trinitrobenzene has a larger molecular size, the binding affinity of 1,3,5-trinitrobenzene on GO is much stronger than that of 1,3,5-trichlorobenzene and 1,3,5-trimethylbenzene (Fig. 3A). Similar trends are shown for hydroxyl- and amino-substituted compounds (*p*-chlorophenol, *p*-chloroaniline, 1-naphthylamine, and 2-naphthol). These polar compounds have slightly larger molecular sizes than their apolar counterparts (*p*-dichlorobenzene and naphthalene) (fig. S2); however, except for 2-naphthol, the binding affinity of the polar compounds on GO is markedly stronger (Fig. 3, B and C), with K_d values over 20 times higher than for the apolar compounds (table S3). The binary-solute sorption experiments provide consistent results that the binding affinity of polar 1-naphthylamine is higher than that of apolar naphthalene (fig. S3G).

Size selectivity of aromatics on oxygen-enriched GO in gas phase

The size-based selective binding on GO is also applicable to molecules in the gas phase. We compared the column binding capacity of GO for toluene and *o*-xylene gas (20% of saturated vapor pressure) at 5 and 75% relative humidity (RH) (Fig. 4). The binding affinity of *o*-xylene is higher than that of toluene at 5% RH, whereas a reversed trend is shown at 75% RH. The binding capacities of toluene and *o*-xylene are 0.034 and 0.042 mmol/g at 5% RH and are 0.040 and 0.018 mmol/g at 75% RH, respectively. The binding selectivity of the small-sized toluene on GO is facilitated by increasing the hydration level of GO.

Mechanisms for size/polarity selectivity of aromatics on oxygen-enriched GO

In previous works, the selective molecular binding of aromatics was commonly achieved on materials with uniform nanosized pores via size exclusion of large molecules (*7*–*12*). However, this mechanism cannot be applied to the observed selectivity trend, considering that GO is a two-dimensional atomic sheet without fixed pores (fig. S1, E and F). We propose that the highly selective binding ability of GO for small aromatic compounds is due to the size match–based selective binding. It is well-recognized that graphitic regions are the main binding sites of carbonaceous materials for aromatic molecules, particularly for apolar aromatic molecules, resulting from a combination of hydrophobic effect and π-π coupling interactions (*17*, *18*, *33*–*37*). For the tested GO, the major binding sites are isolated, small-sized graphitic regions (2.5 to 5.6 nm) separated by oxygen-containing aliphatic carbons. In the aqueous phase, the size of accessible graphitic regions is further reduced because of the

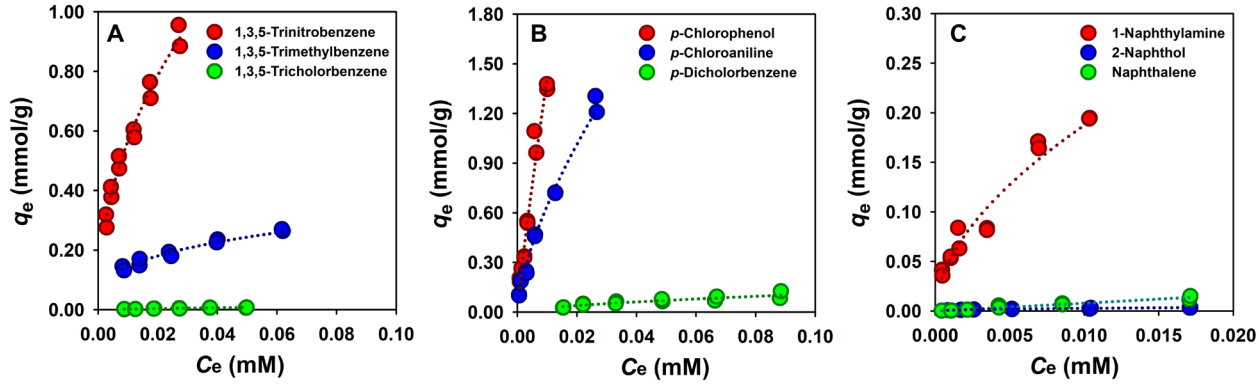

Fig. 3. Binding affinity of aromatics with different polarity on GO in the aqueous phase. Adsorption isotherms plotted as adsorbed concentration (q_e) against aqueous-phase concentration (C_e) at equilibrium for (**A**) 1,3,5-substituted benzenes, (**B**) *p*-substituted benzenes, and (**C**) naphthalene and substituted naphthalene. The experiments were conducted using a batch approach at ambient temperature. All adsorption data were collected in duplicate.

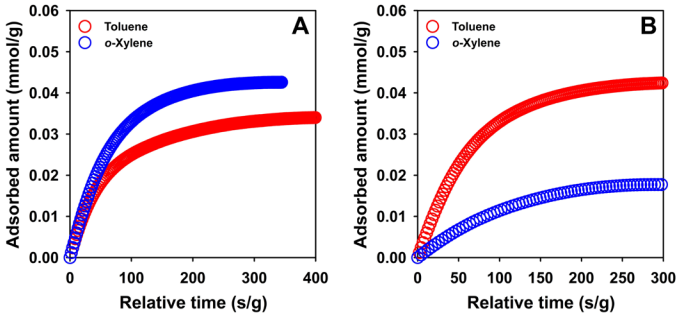

Fig. 4. Binding affinity of aromatics on GO in the gas phase. Gas-phase adsorption curves of toluene and *o*-xylene (20% of saturated vapor pressure) at RH of (**A**) 5% and (**B**) 75%. The experiments were performed in column mode at ambient temperature and pressure using helium as the carrier and balance gas.

hydration of the surrounding oxygen-containing groups (epoxies and hydroxyls) (*38*). The hydration of GO is confirmed by the ^{1}H NMR analysis results. The ^{1}H NMR spectra of GO exhibit a strong ^{1}H NMR signal (fig. S4). Given that GO itself has a very low hydrogen concentration, this signal must be assigned to water in the sample. The observed chemical shift of around 6 ppm is characteristic of water molecule with enhanced hydrogen bonding. The relaxation behavior evidenced by this signal shows that it can be attributed to dynamically bound rather than free water (*39*). For instance, unlike other ^{1}H NMR signals resolved at 0.5, 13.5, and 16.5 ppm after long $T_{1\rho}$ filter times ($T_{1\rho}$ refers to the spin-lattice relaxation time in the rotating frame), the dominant ^{1}H NMR signal is not narrowed by 12.5-kHz magic angle spinning (MAS), indicating that it derives from a molecule with strong ^{1}H—^{1}H dipolar couplings, as found in more or less immobilized water molecules. A series of spectra in fig. S4 document that the broad signal exhibits very fast $T_{1\rho}$ relaxation on the time scale of 0.05 ms, indicating large-amplitude dynamics with rates near the $T_{1\rho}$ minimum, on the order of pulse field strength (i.e., $|\gamma B_1| = 3 \times 10^5$/s) (*40*), corresponding to rotation correlation times near 3 μs. The rotation correlation time of water bound on GO is six orders of magnitude longer than that of bulk liquid water (*41*) and is in a similar order to that reported for structural water in proteins (*42*) and hydrogels (*43*). The result indicates the strong and irreversible interactions of the water molecules with the GO surface.

We postulate that the water molecules attached to the oxygen groups decrease the effective size of the graphitic regions to a size dimension slightly larger than one benzene ring in aqueous phase. The sizes of the small-sized aromatic compounds tested in this work match the size of the graphitic regions, leading to strong binding. On the other hand, the graphitic regions of GO are not accessible for the large aromatic compounds (i.e., naphthalene, phenanthrene, and most multisubstituted benzenes) because of the steric hindrance effect (see the schematic description in fig. S5). The modulation of the size of graphitic regions by oxygen group–dependent hydration also explains the selective binding of toluene over *o*-xylene in gas-phase adsorption at high RH. The increase in RH increased the hydration level of GO and consequently decreased the exposed surface areas of graphitic regions, leading to enhanced steric hindrance and, in turn, higher selectivity for (smaller) toluene. Compared with the methyl-substituted benzenes, the steric hindrance effect is more prominent for choloro-substituted benzenes. Despite their higher hydrophobicity, *p*-dichlorobenzene and 1,3,5-trichlorobenzene exhibit markedly lower binding affinity than *p*-xylene and 1,3,5-trimethylbenzene, respectively (table S3). This is first due to the smaller molecular sizes of *p*-xylene and 1,3,5-trimethylbenzene. Furthermore, the methyl group is relatively flexible compared to the chlorine atom, which may further alleviate the steric hindrance by optimizing the position of the attached hydrogen atoms. In addition, the hydrogen atoms in the methyl group can interact with the graphitic regions of GO via π-H interaction (*44*, *45*), facilitating the binding of methyl-substituted benzenes. The π-H interaction also explains the enhanced binding affinity of *m*-xylene and *p*-xylene than *o*-xylene. The ortho-orientation of methyl groups markedly limits their rotation, inhibiting the π-H interaction of methyl hydrogens with GO. Notably, the K_d values of *m*-xylene and *p*-xylene are appropriately six and nine times higher than that of *o*-xylene, indicating that GO is able to effectively separate xylene isomers in the aqueous solution. For dichlorobenzenes that cannot induce π-H interaction with the graphitic regions of GO, *p*-dichlorobenzene exhibited a lower binding affinity than the other two isomers because of its larger molecular size.

Unlike apolar compounds, polar compounds can induce hydrogen bonding and polar interactions with the oxygen groups (e.g., epoxies and hydroxyls) on GO despite relatively low hydrophobicity. In addition, such compatibility of the polar groups of molecules

with the oxygen groups on GO can provide extra binding space by minimizing the steric hindrance limit of the neighboring graphitic region, therefore leading to enhanced binding. Thus, the molecular size and polarity of compounds are both key determinants of the binding selectivity by GO. Now, molecular size–based selectivity is mostly accomplished on zeolite and molecular imprinting. The molecules are adsorbed inside the zeolite via configurational diffusion if their molecular diameters match the pore dimension of zeolite. Hence, the high size selectivity of the zeolite is commonly accompanied with very slow adsorption kinetics (*8*). Molecularly imprinted polymers can gain molecular selectivity on the basis of both molecular size/shape and functional groups. However, this approach still faces several challenges including template leakage, limited selectivity in aqueous systems, and slow mass transfer within interior surface (*46*). In contrast, GO offers fast kinetics, owing to its open surface without pore structure. The GO can be supported on inorganic particles to avoid unintended aggregation in aqueous phase, further increasing the binding capacity and kinetics (*47*).

To further examine the proposed mechanism of the observed molecular binding selectivity, we simulated the binding interactions of benzene, naphthalene, phenanthrene, toluene, *o*-xylene, and *p*-xylene with a model GO (M-GO; $C_{282}H_{226}O_{173}$) using DFT calculations. The M-GO has 36% of aromatic carbon and 64% of oxidized carbon (5% of C—O—C and 59% of C—OH) (Fig. 5A), and it has a graphitic region size of approximately 2.0 nm, generally consistent with the observations by ^{13}C NMR and HR-TEM. In the absence of water, the optimized geometries of the complexes of M-GO and all six tested compounds are in the face-to-face orientation with a distance of about 0.34 nm to form π-π overlap dispersion. The gas-phase interaction energy with M-GO (Δ*E*) is calculated to be 9.4 kcal/mol for benzene, 15.3 kcal/mol for naphthalene, and 19.3 kcal/mol for phenanthrene, which correlates well with compound's molecular size. A consistent trend is shown for toluene and xylenes (toluene, 11.2 kcal/mol; *p*-xylene, 12.7 kcal/mol; *o*-xylene, 13.1 kcal/mol). These results indicate that, in the absence of water, GO preferentially binds larger molecules without inducing a steric hindrance effect.

M-GO can strongly bind water molecules (average Δ*E* of 4.2 kcal/mol per water molecule) to form water clusters around the oxygen-containing groups, agreeing with the ^1H NMR results. This decreases the size of the graphitic regions on M-GO to 1.4 nm in the presence of three water clusters $(H_2O)_n$ ($n = 10$) (Fig. 5B). Benzene is still able to form a face-to-face complex with the hydrated M-GO with a distance of 0.34 nm and a Δ*E* of 18.7 kcal/mol. In contrast, because of the strong steric hindrance caused by the associated water clusters, the two large-sized PAHs are far away from the surface of hydrated M-GO (at a distance of 0.94 nm for naphthalene and 1.21 nm for phenanthrene), reflecting negligible binding interactions. The Δ*E* of toluene (14.6 kcal/mol) with hydrated M-GO is higher than the Δ*E* of *p*-xylene (13.8 kcal/mol) and *o*-xylene (14.1 kcal/mol). A significant positive correlation ($R^2 = 0.702$, $P = 0.037$) exists between the measured $\log K_d$ and the DFT-calculated Δ*E* with hydrated M-GO for the tested apolar aromatic solutes (fig. S6A). In contrast, a negative correlation ($R^2 = 0.655$, $P = 0.051$) was observed between $\log K_d$ and $\log K_{OW}$ for these solutes (fig. S6B). These correlations confirm the preferential adsorption of smaller and less hydrophobic aromatics on hydrated GO. The deviation of the correlation between $\log K_d$

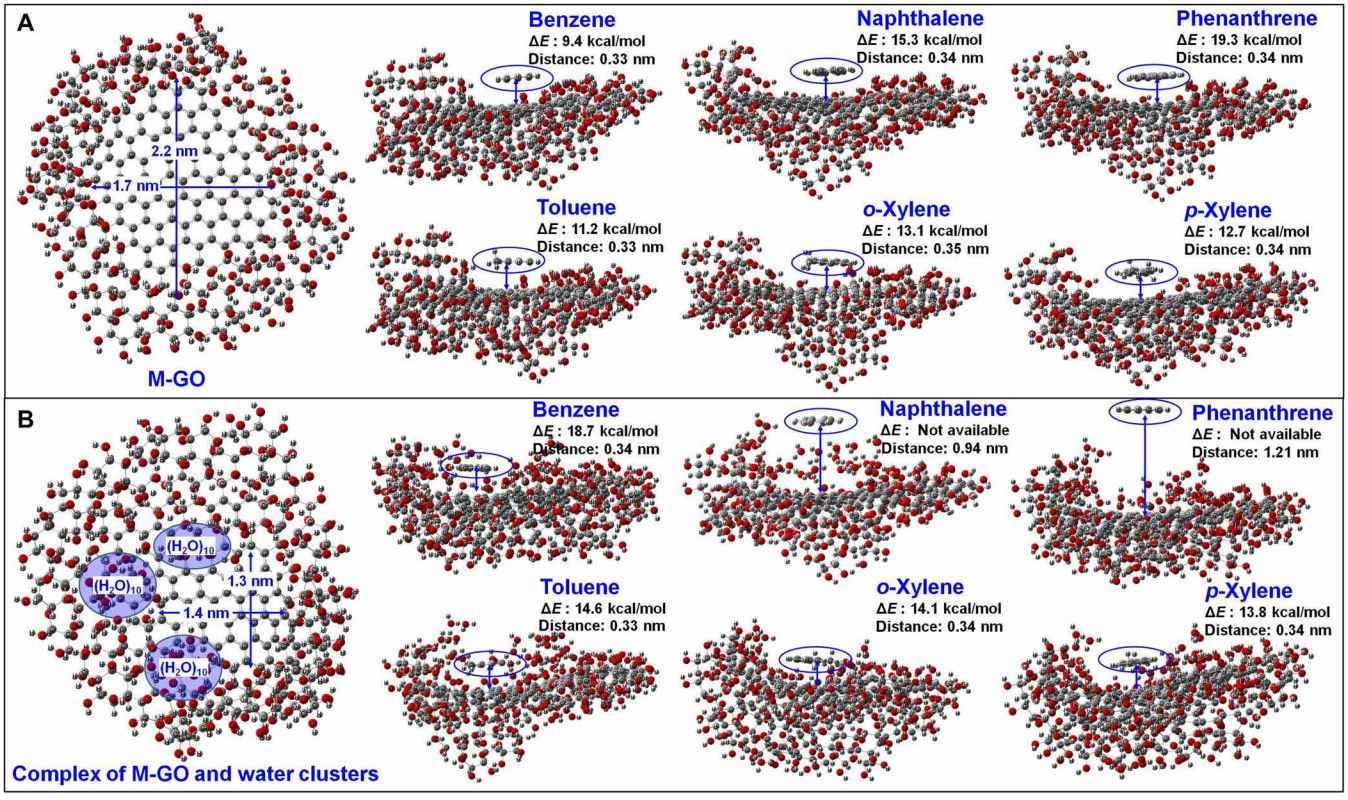

Fig. 5. Theoretical insight into the mechanism for GO selectivity. Optimized geometries and energies of M-GO ($C_{282}H_{226}O_{173}$) interacting with different molecules in the (**A**) absence and (**B**) presence of three water clusters [$(H_2O)_n$, $n = 10$]. The left-hand and right-hand sides display the top view and the side view of the M-GO, respectively.

and ΔE is mostly caused by the higher ΔE of *o*-xylene, probably due to the unpredicted steric effect on the π-H interaction. This reflects a slightly overpredicted size of the graphitic region (serving as the binding site) on hydrated M-GO, which is likely due to the lower hydration degree (with only three water clusters) in the simulation. Nonetheless, the DFT calculations support our proposed size match–based selective binding mechanism of GO. To further examine the role of GO hydration in its selectivity, we investigated the binding of selected aromatics (toluene, *o*-xylene, 1,3,5-trimethylbenzene, chlorobenzene, *o*-dichlorobenzene, and 1,3,5-trichlorobenzene) to reduced GO (RGO). In contrast to GO, RGO exhibited higher binding affinity for larger and more hydrophobic aromatics (e.g., highest for 1,3,5-trichlorobenzene), and the $\log K_d$ values were significantly correlated with $\log K_{OW}$ values ($R^2 = 0.981$, $P = 0.0001$; fig. S7). This suggests that the graphitic regions of RGO are accessible for both small and large molecules without effective surrounding hydration layers due to the low content (16 at %; determined by XPS) of oxygen-containing functional groups. Thus, the highly selective binding of GO toward apolar aromatics is enhanced by oxygen group–dependent hydration, which decreases the size of graphitic regions.

DISCUSSION

We found that graphene nanosheets can achieve high size/polarity selectivity for targeted aromatic molecules in aqueous solution and gas phase by properly grafting oxygen functional groups on the basal plane. Molecular selectivity is primarily imparted by a previously unidentified mechanism based on size match interactions of the aromatic molecules and the isolated graphitic regions, which is tuned by the encompassing oxygen-containing functional groups on the graphene nanosheets. For aromatics with similar sizes, polar aromatics are selectively bound on GO over apolar ones, owing to the complementarity of their polar groups with the oxygen-containing groups of GO. Therefore, unlike most adsorbents that preferentially bind larger and more hydrophobic aromatics, this material selectively accomplishes the opposite. Our findings provide opportunities for precision separation and molecular recognition enabled by size/polarity match–based selectivity, which have important implications in various fields including separation technology, selective catalysis, sensors, and drug delivery.

MATERIALS AND METHODS

Materials

The aromatic compounds used in this study included benzene (99.5%; Shanghai Lingfeng Chemical Reagent Co. Ltd., China), naphthalene (99%; Sigma-Aldrich), phenanthrene (98%; Sigma-Aldrich), 1-naphthylamine (98%; Sigma-Aldrich), 2-naphthol (99%; Sigma-Aldrich), chlorobenzene (99.0%; Shanghai Lingfeng Chemical Reagent Co. Ltd.), *o*-dichlorobenzene (99%; J&K Chemical, China), *m*-dichlorobenzene (97%; Sigma-Aldrich), *p*-dichlorobenzene (99.5%; Fluka, Switzerland), 1,2,4-trichlorobenzene (99.0%; Fluka), 1,3,5-trichlorobenzene (99%; Supelco, USA), *p*-chlorophenol (99%; Alfa Aesar, USA), *p*-chloroaniline (98%; Nanjing Chemical Reagent Co. Ltd., China), toluene (99.5%; Nanjing Chemical Reagent Co. Ltd), *o*-xylene (98.0%; Supelco), *m*-xylene (99.5%; Sigma-Aldrich), *p*-xylene (99.5%; Sigma-Aldrich), 1,3,5-trimethylbenzene (97%; Macklin, China), nitrobenzene (99.5%; Fluka), *m*-dinitrobenzene (97%; Sigma-Aldrich), and 1,3,5-trinitrobenzene (99.9%; Sigma-Aldrich). GO (99.0%) and RGO (98.9%) were purchased from XFNANO Materials Tech (China). GO was prepared by the modified Hammers method (*18*, *23*) and was mainly in the form of nanosheets with a diameter of 0.5 to 5 μm and thickness of 0.8 to 1.2 nm (according to the information provided by the manufacturer). RGO was prepared by the reduction of GO using L-ascorbic acid (*48*). All these materials were used without further purification.

Characterization of GO

HR-TEM images of GO were collected on a Titan G2 60-300 spherical aberration–corrected TEM (FEI, USA) equipped with a high-brightness Schottky field emission gun and an image aberration corrector to provide a spatial resolution better than 0.8 Å in TEM mode. Solid-state NMR spectra were recorded using a Bruker AVANCE III 400 NMR spectrometer equipped with a 4-mm MAS probe (Bruker, Massachusetts, USA) and were operated at 400- and 100-MHz resonance frequency for ^{1}H and ^{13}C, respectively. All spectra were collected at 12.5 kHz and at ambient temperature. The ^{13}C direct polarization NMR spectrum was collected with 4-μs excitation pulse, 1- or 5-s recycle delay, and 4096 scans. ^{1}H NMR spectra were measured after a spin lock at a field strength of $|\gamma B_1| = 50$ kHz for durations up to 3.2 ms, probing $T_{1\rho}$ of different ^{1}H NMR signals. The ^{1}H and ^{13}C chemical shift was referenced to hydroxyapatite peak at 0.18 ppm and carbonyl peak of freshly made crystalline glycine at 176.49 ppm.

Aqueous-phase batch adsorption

The isotherm experiment was conducted in the single-solute mode using a batch adsorption test described in our previous studies (*19*, *21*). To initiate the experiment, an aqueous solution of GO (5 mg/liter) was prepared by ultrasonication and was added to a 40-ml Amber U.S. Environmental Protection Agency vial with polytetrafluoroethylene (PTFE)–lined screw cap. Afterward, a stock solution of adsorbate prepared in methanol was added to the vial, and the volume percentage of methanol was kept below 0.1% to minimize cosolvent effects. The initial concentration ranges were 0.0003 to 0.0200 mM for benzene and PAHs, 0.006 to 0.150 mM for chloro-substituted benzenes, 0.01 to 0.50 mM for methyl-substituted benzenes, 0.004 to 0.060 mM for nitro-substituted benzenes, 0.0008 to 0.0100 mM for *p*-chlorophenol, 0.001 to 0.030 mM for *p*-chloroaniline, 0.0006 to 0.0100 mM for 1-naphthylamine, and 0.0008 to 0.0200 mM for 2-naphthol. The samples were covered with aluminum foil and end-over-end mixed at ambient temperature for 72 hours to reach apparent adsorption equilibrium. At the end of adsorption experiment, an aliquot of the samples was withdrawn and was filtered through a 0.22-μm PTFE membrane (Anpel Scientific Instrument, China) to remove the dispersed GO (*49*). The adsorbate concentrations in the filtrates were analyzed by high-performance liquid chromatography (detailed analytical methods can be found in the Supplementary Materials). To account for solute loss from processes other than adsorbent adsorption, calibration curves were built separately from control samples receiving the same treatment as the adsorption samples but no GO. On the basis of the obtained calibration curves, the adsorbed mass of the solute was calculated by subtracting the mass in the aqueous phase from the mass added. The equilibrium pH (buffered with 0.05 M tris-HCl), as measured at the end of the adsorption experiments, was approximately 7.5. A separate set of experiments were conducted to test the binding selectivity of GO in binary-solute systems. These tests were performed by single-point adsorption (*50*) at the initial

concentrations of 0.005 mM for solutes in the benzene/phenanthrene system, 0.07 mM for solutes in the methyl-substituted benzene systems, and 0.01 mM for solutes in the rest of the binary-solute systems. The single-solute binding affinity of different aromatics on RGO was investigated using the single-point adsorption approach at a fixed initial solute concentration (0.02 mM). Duplicate samples were prepared for the isotherm experiments, and triplicate samples were prepared for single-point adsorption experiments.

Gas-phase column adsorption

Gas-phase column adsorption experiments were conducted with toluene and *o*-xylene on GO at different RH, using a BSD-MAB multiconstituent adsorption breakthrough curve analyzer (Beishide Instrument, China). Tests were run at ambient temperature and pressure using helium as the carrier and balance gas. The vapor concentration of the adsorbates was set at 20% of the saturated vapor pressure. More detailed operating parameters can be found in the Supplementary Materials.

DFT calculation

The molecular interaction energies of an M-GO ($C_{282}H_{226}O_{173}$) with water clusters [$(H_2O)_n$, n = 10] and different molecules were calculated using the Gaussian 09(5) program (*51*) at the M062x/6-31g(d,p)(4) level (*52*).

SUPPLEMENTARY MATERIALS

Supplementary material for this article is available at https://science.org/doi/10.1126/sciadv.abn4650

REFERENCES AND NOTES

1. N. Y. Chen, W. E. Garwood, F. G. Dwyer, *Shape Selective Catalysis in Industrial Applications* (Marcel Dekker, 1996).
2. L. Chen, P. S. Reiss, S. Y. Chong, D. Holden, K. E. Jelfs, T. Hasell, M. A. Little, A. Kewley, M. E. Briggs, A. Stephenson, K. M. Thomas, J. A. Armstrong, J. Bell, J. Busto, R. Noel, J. Liu, D. M. Strachan, P. K. Thallapally, A. I. Cooper, Separation of rare gases and chiral molecules by selective binding in porous organic cages. *Nat. Mater.* **13**, 954–960 (2014).
3. H. Yang, B. Yuan, X. Zhang, Supramolecular chemistry at interfaces: Host-guest interactions for fabricating multifunctional biointerfaces. *Acc. Chem. Res.* **47**, 2106–2115 (2014).
4. J. Y. S. Lin, Molecular sieves for gas separation. *Science* **353**, 121–122 (2016).
5. H. G. Franck, J. W. Stadelhofer, *Industrial Aromatic Chemistry* (Springer, 1988).
6. D. S. Sholl, R. P. Lively, Seven chemical separations to change the world. *Nature* **532**, 435–437 (2016).
7. M. E. Davis, Ordered porous materials for emerging applications. *Nature* **417**, 813–821 (2002).
8. J. Pérez-Ramírez, C. H. Christensen, K. Egeblad, C. H. Christensen, J. C. Groen, Hierarchical zeolites: Enhanced utilisation of microporous crystals in catalysis by advances in materials design. *Chem. Soc. Rev.* **37**, 2530–2542 (2008).
9. H. Furukawa, K. E. Cordova, M. O'Keeffe, O. M. Yaghi, The chemistry and applications of metal-organic frameworks. *Science* **341**, 1230444 (2013).
10. A. G. Slater, A. I. Cooper, Function-led design of new porous materials. *Science* **348**, aaa8075 (2015).
11. K. Adil, Y. Belmabkhout, R. S. Pillai, A. Cadiau, P. M. Bhatt, A. H. Assen, G. Maurin, M. Eddaoudi, Gas/vapour separation using ultra-microporous metal-organic frameworks: Insights into the structure/separation relationship. *Chem. Soc. Rev.* **46**, 3402–3430 (2017).
12. Z. Wang, S. Zhang, Y. Chen, Z. Zhang, S. Ma, Covalent organic frameworks for separation applications. *Chem. Soc. Rev.* **49**, 708–735 (2020).
13. J. Kong, N. R. Franklin, C. Zhou, M. G. Chapline, S. Peng, K. Cho, H. Dai, Nanotube molecular wires as chemical sensors. *Science* **287**, 622–625 (2000).
14. N. L. Rosi, C. A. Mirkin, Nanostructures in biodiagnostics. *Chem. Rev.* **105**, 1547–1562 (2005).
15. M. Trojanowicz, Analytical applications of carbon nanotubes: A review. *TrAC-Trend. Aanl. Chem.* **25**, 480–489 (2006).
16. W. Yang, K. R. Ratinac, S. P. Ringer, P. Thordarson, J. J. Gooding, F. Braet, Carbon nanomaterials in biosensors: Should you use nanotubes or graphene? *Angew. Chem. Int. Ed.* **49**, 2114–2138 (2010).
17. M. S. Mauter, M. Elimelech, Environmental applications of carbon-based nanomaterials. *Environ. Sci. Technol.* **42**, 5843–5859 (2008).
18. F. Perreault, A. F. de Faria, M. Elimelech, Environmental applications of graphene-based nanomaterials. *Chem. Soc. Rev.* **44**, 5861–5896 (2015).
19. W. Chen, L. Duan, L. Wang, D. Zhu, Adsorption of hydroxyl-and amino-substituted aromatics to carbon nanotubes. *Environ. Sci. Technol.* **42**, 6862–6868 (2008).
20. Y. Shen, B. Chen, Sulfonated graphene nanosheets as a superb adsorbent for various environmental pollutants in water. *Environ. Sci. Technol.* **49**, 7364–7372 (2015).
21. L. Zuo, Y. Guo, X. Li, H. Fu, X. Qu, S. Zheng, C. Gu, D. Zhu, P. J. J. Alvarez, Enhanced adsorption of hydroxyl-and amino-substituted aromatic chemicals to nitrogen-doped multiwall carbon nanotubes: A combined batch and theoretical calculation study. *Environ. Sci. Technol.* **50**, 899–905 (2016).
22. L. Wang, D. Zhu, J. Chen, Y. Chen, W. Chen, Enhanced adsorption of aromatic chemicals on boron and nitrogen co-doped single-walled carbon nanotubes. *Environ. Sci. Nano* **4**, 558 (2017).
23. W. S. Hummers Jr., R. E. Offeman, Preparation of graphitic oxide. *J. Am. Chem. Soc.* **80**, 1339 (1958).
24. C. Liu, T. Wu, P.-C. Hsu, J. Xie, J. Zhao, K. Liu, J. Sun, J. Xu, J. Tang, Z. Ye, D. Lin, Y. Cui, Direct/alternating current electrochemical method for removing and recovering heavy metal from water using graphene oxide electrode. *ACS Nano* **13**, 6431–6437 (2019).
25. N. R. Wilson, P. A. Pandey, R. Beanland, R. J. Young, I. A. Kinloch, L. Gong, Z. Liu, K. Suenaga, J. P. Rourke, S. J. York, J. Sloan, Graphene oxide: Structural analysis and application as a highly transparent support for electron microscopy. *ACS Nano* **3**, 2547–2556 (2009).
26. S. Saha, P. Samanta, N. C. Murmu, T. Kuila, Investigation of the surface plasmon polariton and electrochemical properties of covalent and noncovalent functionalized reduced graphene oxide. *Phys. Chem. Chem. Phys.* **19**, 28588–28595 (2017).
27. T. J. Booth, P. Blake, R. R. Nair, D. Jiang, E. W. Hill, U. Bangert, A. Bleloch, M. Gass, K. S. Novoselov, M. I. Katsnelson, A. K. Geim, Macroscopic graphene membranes and their extraordinary stiffness. *Nano Lett.* **8**, 2442–2446 (2008).
28. C. Gómez-Navarro, J. C. Meyer, R. S. Sundaram, A. Chuvilin, S. Kurasch, M. Burghard, K. Kern, U. Kaiser, Atomic structure of reduced graphene oxide. *Nano Lett.* **10**, 1144–1148 (2010).
29. S. Stankovich, D. A. Dikin, R. D. Piner, K. A. Kohlhaas, A. Kleinhammes, Y. Jia, Y. Wu, S. T. Nguyen, R. S. Ruoff, Synthesis of graphene-based nanosheets via chemical reduction of exfoliated graphite oxide. *Carbon* **45**, 1558–1565 (2007).
30. W. Cai, R. D. Piner, F. J. Stadermann, S. Park, M. A. Shaibat, Y. Ishii, D. Yang, A. Velamakanni, S. J. An, M. Stoller, J. An, D. Chen, R. S. Ruoff, Synthesis and solid-state NMR structural characterization of ^{13}C-labeled graphite oxide. *Science* **321**, 1815–1817 (2008).
31. W. Gao, L. B. Alemany, L. Ci, P. M. Ajayan, New insights into the structure and reduction of graphite oxide. *Nat. Chem.* **1**, 403–408 (2009).
32. S. Park, Y. Hu, J. O. Hwang, E.-S. Lee, L. B. Casabianca, W. Cai, J. R. Potts, H.-W. Ha, S. Chen, J. Oh, S. O. Kim, Y.-H. Kim, Y. Ishii, R. S. Ruoff, Chemical structures of hydrazine-treated graphene oxide and generation of aromatic nitrogen doping. *Nat. Commun.* **3**, 1–8 (2012).
33. S. B. Fagan, A. G. Souza Fiho, J. O. G. Lima, J. M. Filho, O. P. Ferreira, I. O. Mazali, O. L. Alves, M. S. Dresselhaus, 1,2-Dichlorobenzene interacting with carbon nanotubes. *Nano Lett.* **4**, 1285–1288 (2004).
34. T. Kar, H. F. Bettinger, S. Scheiner, A. K. Roy, Noncovalent π-π stacking and CH---π interactions of aromatics on the surface of single-wall carbon nanotubes: An MP2 study. *J. Phys. Chem. C* **112**, 20070–20075 (2008).
35. Z. Zhang, H. Huang, X. Yang, L. Zang, Tailoring electronic properties of graphene by π– π stacking with aromatic molecules. *J. Phys. Chem. Lett.* **2**, 2897–2905 (2011).
36. M. Cao, A. Fu, Z. Wang, J. Liu, N. Kong, X. Zong, H. Liu, J. J. Gooding, Electrochemical and theoretical study of π–π stacking interactions between graphitic surfaces and pyrene derivatives. *J. Phys. Chem. C* **118**, 2650–2659 (2014).
37. E. M. Pérez, N. Martín, π–π interactions in carbon nanostructures. *Chem. Soc. Rev.* **44**, 6425–6433 (2015).
38. A. R. Deline, B. P. Frank, C. L. Smith, L. R. Sigmon, A. N. Wallace, M. J. Gallagher, D. G. Goodwin Jr., D. P. Durkin, D. H. Fairbrother, Influence of oxygen-containing functional groups on the environmental properties, transformations, and toxicity of carbon nanotubes. *Chem. Rev.* **120**, 11651–11697 (2020).
39. K. Schmidt-Rohr, H. W. Spiess, *Multidimensional Solid-State NMR and Polymers* (Academic Press, 1994).
40. V. J. McBrierty, D. C. Douglass, Analysis of NMR relaxation times in polymers with fiber symmetry. *J. Magn. Reson.* **2**, 352–360 (1969).
41. D. Lankhorst, J. Schriever, J. C. Leyte, Determination of the rotational correlation time of water by proton NMR relaxation in $H_2{}^{17}O$ and some related results. *Ber. Bunsen. Phys. Chem* **86**, 215–221 (1982).
42. E. Persson, B. Halle, Nanosecond to microsecond protein dynamics probed by magnetic relaxation dispersion of buried water molecules. *J. Am. Chem. Soc.* **130**, 1774–1787 (2008).

43. A. Yamada-Nosaka, K. Ishikiriyama, M. Todoki, H. Tanzawa, ^{1}H-NMR studies on water in methacrylate hydrogels. I. *J. Appl. Polym. Sci.* **39**, 2443–2452 (1990).
44. K. S. Kim, P. Tarakeshwar, J. Y. Lee, Molecular clusters of π-systems: Theoretical studies of structures, spectra, and origin of interaction energies. *Chem. Rev.* **100**, 4145–4186 (2000).
45. E. C. Lee, D. Kim, P. Jurečka, P. Tarakeshwar, P. Hobza, K. S. Kim, Understanding of assembly phenomena by aromatic-aromatic interactions: Benzene dimer and the substituted systems. *J. Phys. Chem. A* **111**, 3446–3457 (2007).
46. L. Chen, S. Xu, J. Li, Recent advances in molecular imprinting technology: Current status, challenges and highlighted applications. *Chem. Soc. Rev.* **40**, 2922–2942 (2011).
47. Q. Liu, J. Shi, J. Sun, T. Wang, L. Zeng, G. Jiang, Graphene and graphene oxide sheets supported on silica as versatile and high-performance adsorbents for solid-phase extraction. *Angew. Chem.* **123**, 6035–6039 (2011).
48. J. Zhang, H. Yang, G. Shen, P. Cheng, J. Zhang, S. Guo, Reduction of graphene oxide via L-ascorbic acid. *Chem. Commun.* **46**, 1112–1114 (2010).
49. D. A. Dikin, S. Stankovich, E. J. Zimney, R. D. Piner, G. H. B. Dommett, G. Evmenenko, S. T. Nguyen, R. S. Ruoff, Preparation and characterization of graphene oxide paper. *Nature* **448**, 457–460 (2007).
50. X. Zhang, J. Shen, N. Zhuo, Z. Tian, P. Xu, Z. Yang, W. Yang, Interactions between antibiotics and graphene-based materials in water: A comparative experimental and theoretical investigation. *ACS Appl. Mater. Interfaces* **8**, 24273–24280 (2016).
51. M. J. Frisch, G. W. Trucks, H. B. Schlegel, G. E. Scuseria, M. A. Robb, J. R. Cheeseman, G. Scalmani, V. Barone, B. Mennucci, G. A. Petersson, H. Nakatsuji, M. Caricato, X. Li, H. P. Hratchian, A. F. Izmaylov, J. Bloino, G. Zheng, J. L. Sonnenberg, M. Hada, M. Ehara, K. Toyota, R. Fukuda, J. Hasegawa, M. Ishida, T. Nakajima, Y. Honda, O. Kitao, H. Nakai, T. Vreven, J. A. Montgomery Jr., J. E. Peralta, F. Ogliaro, M. Bearpark, J. J. Heyd, E. Brothers, K. N. Kudin, V. N. Staroverov, R. Kobayashi, J. Normand, K. Raghavachari, A. Rendell, J. C. Burant, S. S. Iyengar, J. Tomasi, M. Cossi, N. Rega, J. M. Millam, M. Klene, J. E. Knox, J. B. Cross, V. Bakken, C. Adamo, J. Jaramillo, R. Gomperts, R. E. Stratmann, O. Yazyev, A. J. Austin, R. Cammi, C. Pomelli, J. W. Ochterski, R. L. Martin, K. Morokuma, V. G. Zakrzewski, G. A. Voth, P. Salvador, J. J. Dannenberg, S. Dapprich, A. D. Daniels, Ö. Farkas, J. B. Foresman, J. V. Ortiz, J. Cioslowski, D. J. Fox, *Gaussian 09*, Revision A.02 (Gaussian Inc., 2009).
52. Y. Zhao, D. G. Truhlar, The M06 suite of density functionals for main group thermochemistry, thermochemical kinetics, noncovalent interactions, excited states, and transition elements: Two new functionals and systematic testing of four M06-class functionals and 12 other functionals. *Theor. Chem. Acc.* **120**, 215–241 (2008).
53. R. P. Schwarzenbach, P. M. Gschwend, D. M. Imboden, *Environmental Organic Chemistry* (John Wiley & Sons Inc., 2002).
54. S. Zhang, H. Wang, J. Liu, C. Bao, Measuring the specific surface area of monolayer graphene oxide in water. *Mater. Lett.* **261**, 127098 (2020).

Acknowledgments: Peking University is the first contribution organization of this study. **Funding:** This work was funded by National Natural Science Foundation of China grant 41991331, National Natural Science Foundation of China grant 21920102002, National Natural Science Foundation of China grant 21777002, National Key Research and Development Program of China grant 2019YFC1804201, and U.S. National Science Foundation (NSF) ERC on Nanotechnology-Enabled Water Treatment grant EEC-1449500. **Author contributions:** Conceptualization: D.Z. Methodology: D.Z., S.B., Y.G., L.L., and K.S.-R. Investigation: B.W., Z.Z., S.B., Y.G., L.L., P.D., and J.M. Visualization: H.F., B.W., and P.D. Supervision: D.Z. Writing—original draft: H.F. and X.Q. Writing—interpretation, review, and editing: H.F., D.Z., X.Q., S.Z., K.S.-R., S.T., and P.J.J.A. **Competing interests:** The authors declare that they have no competing interests. **Data and materials availability:** All data needed to evaluate the conclusions in the paper are present in the paper and/or the Supplementary Materials.

Submitted 8 January 2022
Accepted 14 June 2022
Published 29 July 2022
10.1126/sciadv.abn4650